

# The vortex doublet as a generating mechanism of inviscid vortex sheets. Part I: separation at a sharp edge

A. C. DeVoria

Department of Mechanical and Aerospace Engineering, University of Florida, Gainesville,  
FL 32611, USA

K. Mohseni

Department of Mechanical and Aerospace Engineering, University of Florida, Gainesville,  
FL 32611, USA

Department of Electrical and Computer Engineering, University of Florida, Gainesville, FL  
32611, USA

March 20, 2019

## Abstract

In this paper it is proposed that, in two-dimensional flow, the vortex sheet corresponding to inviscid flow separation at a sharp edge is generated by a vortex doublet. The existence of the doublet arises as a result of representing the solid surfaces as vortex doublet sheets. Namely, the inviscid limit of the attached boundary layer and its image layer inside the surface comprise the doublet sheet. The sheet strength represents the amount of circulation in the boundary layer and the net strength of interacting layers at the sharp edge relates to the circulation to be shed into the fluid. This net strength is a global quantity that represents instant communication of changes in the flow to the shedding point. The shedding of a vortex sheet is interpreted as the doublet sheet being ‘torn apart,’ such that one layer is the vortex sheet shed into the fluid and the other layer is the image of this sheet inside the surface. The unsteady Kutta condition is manifested by requiring that the strength of the doublet be such that it induces a flow that instantaneously and mutually neutralizes itself with the singular pressure gradient of the flow attempting to navigate around the sharp edge. The neutralization of the pressure gradient is accomplished by the inviscid generation of vorticity at the edge and is also the mechanism that tears apart the doublet. These results are obtained at the level of the Euler equation (momentum) instead of Bernoulli’s equation (energy). As such, there is a finite force exactly at the sharp edge that is associated with the inviscid generation of vorticity and is proportional to the time rate-of-change of the doublet strength. Furthermore, this force corresponds to an ‘acceleration reaction’ of the fluid that is impulsively accelerated as it passes the sharp edge, which in turn communicates an instantaneous change in the total kinetic energy of the fluid to infinity. When the solid surface is a finite body, this force has a finite value even for an infinite impulsive acceleration of the body. Example simulations are presented for validation of the derived shedding equations for the angle, velocity and rate of shed circulation of the vortex sheet at the edge.

## 1 Introduction

This paper is the first in a two-part series that investigates the shedding mechanism of inviscid two-dimensional vortex sheets. Part I focuses on the case of shedding occurring from a sharp edge so that the separation location is fixed by this geometry. In Part II the more general case of separation from a smooth surface is considered, where the separation location is not fixed, but is allowed to move along the

surface. This seemingly minor difference results in several important nuances that deepen the analysis. Part II also presents an inviscid model for predicting the separation location, in addition to the modification of the shedding equations for the vortex sheet derived in Part I.

Modeling separated flow has long been a challenging interest in the general fluid dynamics community. Great advances in computational power and techniques have made tackling the problem via direct numerical simulation of the Navier-Stokes equations more feasible. The historical alternative is the high-Reynolds number assumption whereby free shear layers and boundary layers are represented by infinitely thin vortex sheets. Calculation of the dynamics of vortex sheets, governed by the Birkhoff-Rott equation, is not without difficulty however. Simplification of the numerical evaluation of the governing equations is obtained by discretizing a vortex sheet into point vortices, a technique that dates back to [37] and [44] in the 1930s and represents the beginning of what is now referred to as vortex methods [24]. The discretization, however, invites new issues of convergence that often result in chaotic motion of the point vortices [14]. The vortex blob method developed by [5] and championed by Krasny & coworkers [e.g., 22, 23, 30] is a general means of regularization via a smoothing parameter that is thought to represent the physical effects of viscosity. This method is very useful and perhaps necessary for the numerical stability of large-time calculations of vortex sheet dynamics [34, 19]. Nevertheless, with the aid of computers, multi-vortex shedding models have become commonplace [e.g., 6, 40, 20, 7, 16, 8, 28, 46, 43]. However, one fundamental issue with these methods is the proper introduction of new vorticity as the equations of motion are singular at the initialization of a point vortex at a sharp edge (see Appendix B for more).

The velocity field induced by a vortex sheet is governed by the inviscid Euler equations. For a vortex sheet having a strength density  $\gamma(s, t)$ , the problem can be transformed by letting  $\Gamma(s, t)$  be a Lagrangian parameter describing the amount of circulation in the sheet as measured from a reference point with coordinate  $s$ . The strength density of the sheet is  $\gamma(s, t) = \partial\Gamma/\partial s$ . For a location  $z = x + iy$  not on the sheet, the induced complex conjugate velocity can be written as:

$$u - iv = \frac{\partial \bar{z}}{\partial t} = \frac{dw_o}{dz} + \frac{1}{2\pi i} \int \frac{\gamma(s)ds}{z - z(s)}, \quad (1)$$

where  $z(s)$  is the sheet location and  $w_o(z)$  is an external potential due to all agencies besides the sheet. [36] (among others) reduced the problem to a similarity solution and computed the self-similar shape of a rolled-up semi-infinite free vortex sheet as well as the shapes of vortex sheets shed from the apex of infinite wedges. [19] has carefully computed the truly unsteady vortex sheet shedding from the cusped edges of moving, finite flat plates where the plate was also represented as a vortex sheet of known geometry. For simplicity we are here considering a single vortex sheet being shed into the fluid, but the integral in (1) can more generally be considered as integration over the union of all sheets present [29]. This equation is kinematical as well as dynamical as it ensures continuity of pressure everywhere across the sheet including the shedding edge [see e.g. 14]. When  $z$  is a point on the sheet then, with the implication of the Cauchy principal value, the above integral becomes the Birkhoff-Rott equation. Recently, [11] proposed a model of the local self-induced velocity of a vortex sheet that allows integration through the singularity of this equation and helps stabilizes the roll-up without a regularizing kernel.

Regardless of the shedding problem under consideration or its formulation, an additional constraint of a bounded flow at the shedding edge is also required; this is the famous Kutta condition. The steady Kutta condition of classical aerodynamics determines the bound circulation around an airfoil such that the geometric mapping singularity at the sharp trailing edge is canceled by a stagnation point in the virtual plane. In unsteady cases, the flow is still required to be regular and the Kutta condition physically relates to the rate of circulation generation/shedding from the edge. [41] determined an equation by considering the vorticity flux into a shedding viscous shear layer to give:

$$\frac{d\Gamma}{dt} = \frac{1}{2}(u_-^2 - u_+^2),$$

where  $\Gamma$  is the circulation in the shear layer of finite thickness,  $u_+$  and  $u_-$  are velocities just above and below the layer. [3] derived a similar result from Bernoulli's equation and with the assumption that there is no pressure difference at the edge so that the inviscid form of the above equation may be written as:

$$\frac{d\Gamma_s}{dt} = u_s \gamma_s, \quad (2)$$

where  $\Gamma_s$  is the circulation shed into the vortex sheet of zero thickness,  $u_s = \frac{1}{2}(u_- + u_+)$  is the shedding velocity tangential to the vortex sheet, and  $\gamma_s = (u_- - u_+)$  is again the sheet strength density. [3] conclude that the shedding angle of the vortex sheet is tangential to one of the edge faces (dependent on the sign of shed circulation), which is based on the works of [15] and [27] (henceforth referred to as the Giesing-Maskell model of separation). The most glaring criticism of this model is the incompatibility with the steady-state case where the flow leaves the edge along the bisector angle [32]. An in-depth discussion of this result is given in §5 where it will be contextually more relevant.

[47] recently studied the formation of vortex sheets at the trailing edge of airfoils and showed that the vortex sheet may shed at any angle  $\theta_s$  between the two tangential limits of parallel to the edge faces. They argued that a vortex sheet, in and of itself, is inadequate to describe the viscous shear layer flow in a dynamic sense because the sheet only conserves the tangential jump in velocity across the sheet. As such, the mass and momentum within the shear layer are not explicitly taken into account. They applied conservation laws to a wye-shaped control volume encompassing the two boundary layers approaching the trailing edge that merge and create the free shear layer that is shed into the fluid. Upon taking the inviscid limit, they were able to derive an equation for the angle of a shedding vortex sheet. The result showed a continuous variation of this angle between the limits of the Giesing-Maskell model, and also includes the steady-state case. Inspired by this, they also proposed a generalized sheet to properly model viscous shear layers. Namely, the conventional vortex sheet with a jump in tangential velocity representing the circulation per-unit-length within the layer can be superimposed with sheets that have jumps in other physical quantities, for example a jump in the stream function representing the amount of mass entrainment in the shear layer.

This paper also focuses on the formation of two-dimensional inviscid vortex sheets shed from sharp edges. The novelty here is the introduction of a vortex doublet as the generation mechanism that offers further elucidation of the physics of vorticity generation. The paper is organized as follows. In §2 we present the concept of a vortex doublet sheet as an inviscid representation of a solid surface and the vorticity/circulation within an attached boundary layer. §3 discusses the specifics of how the interaction of the vortex doublet sheets at the sharp edge relates to the circulation to be shed. §4 presents the physics of inviscid vorticity generation with mathematical support. §5 derives the equations for the shedding angle and velocity, and the rate of shed circulation. Then §6 presents example simulations as validation of the shedding equations.

## 2 Vortex doublet sheet

This section begins with a brief discussion of conventional representations of surfaces satisfying the no through-flow condition. The purpose is to show how the associated concepts can naturally be extended to a representation of a solid surface that we call a *vortex doublet sheet* and that has a specific physical meaning with regard to the vorticity generated along such a surface. This discussion is largely qualitative with supporting derivations and mathematical discussions given in the subsequent sections.

In computing (1) one has several options for describing different contributions to the flow. These options are mainly distinguished by the representation of the solid surface(s) from which vorticity is shed. In classical potential flow, the method of images is often employed where all singularities in the flow have ‘images’ inside the solid such that the no through-flow condition on the surface is satisfied. However, this technique requires conformal mappings of the geometry to virtual planes where image systems are known (e.g. mirror image, circle theorem), which can be restrictive for more complex geometries in the physical plane. Alternatively, the surface can be replaced with a vortex sheet whose strength density  $\gamma$  is determined by satisfying the no through-flow condition. If the potential slip flow on the surface is known, then  $\gamma$  can also be determined by ‘satisfying’ the no-slip condition (e.g. see chapter 5.4 of [4] or [26]).

Another choice of representing the surface is through a distribution of dipoles on the surface, which is also known as a ‘double layer’ or simply a ‘dipole sheet/distribution’ [21, 29] and is also a well-developed method of classical potential flow. Dipole sheets have particular utility in the representation of free surfaces, such as in the study of water waves [2, 18], where the sheet strength  $\mu$  is determined from the no-penetration condition, which leads to an evolution equation in the form of a Fredholm integral. Interestingly, the vortex sheet and the dipole sheet are conceptually interchangeable and with the strength density of the former being obtained from a tangential derivative of the latter:  $\gamma = \partial\mu/\partial s$  [for the three-dimensional case see 18]. Stated differently, the vortex sheet strength is obtained as the difference in tangential velocity across

the surface and the dipole sheet strength is obtained as the difference in potential across the surface. [13] recently employed both representations in their derivation of the vortex sheet strength distributions of the classical Sears, Küssner, Theodorsen, and Wagner aerodynamics problems.

The vortex sheet and dipole sheet representations are the foundations for panel methods often used to represent arbitrarily-shaped airfoils. [35] gives an excellent derivation and discussion of these methods. With these surface representations, the no through-flow condition and continuity of the normal velocity across the surface lead to the result that the flow inside the airfoil vanishes relative to a reference frame moving with the body [see also chapter 2.7 of 4]). The meaning of this is that images are not required to maintain the surface as the no through-flow condition is satisfied by definition of the sheet strength  $\mu$ . As such, this zero Neumann boundary condition can be replaced with a Dirichlet condition given by a constant harmonic potential and stream function inside the surface. In the source-dipole panel method for airfoils, the Kutta condition can be employed by supplementing the panels with a point vortex at the sharp trailing edge [35]. A more physical alternative is to superimpose on the source-dipole distribution a vortex sheet of constant strength [e.g. 3], which essentially represents the bound circulation as would be induced by a point vortex at the center of the virtual circle plane (provided a mapping can be found).

Now we present the alternative interpretation of the dipole sheet representation of the surface that we call a vortex doublet sheet. Typically, the dipole sheet is thought of as a distribution of source dipoles. Mathematically, the vortex doublet sheet is distinguished from the source-dipole distribution by the orientation of the singularities. Namely, the source dipoles are oriented tangential to the surface, whereas the vortex doublets are oriented normal to the surface. We adopt the term doublet in place of dipole to reflect that the harmonic functions of the potential have a dipole spatial distribution, not the vorticity. However, there is also significant physical difference associated with the vortex doublet sheet. To this end, consider a viscous flow over a solid surface with an attached boundary layer of thickness  $\delta$ ; for simplicity let the surface be just a flat wall. In the inviscid limit of  $\delta \rightarrow 0$  the vorticity  $\omega$  in the boundary layer becomes infinite and we obtain a vortex sheet. Next, we temporarily borrow the concept of images and presume this vortex sheet to have an image of opposite sign just inside the surface. Then, these two vortex sheets merge to create the vortex doublet sheet of strength (with slight abuse of notation)  $\mu \equiv \lim_{A \rightarrow 0}(\omega A)$ , where  $A = s\delta$  is an infinitesimal area occupied by the infinite vorticity. Hence,  $\mu$  represents the amount of circulation  $\Gamma$  carried in the vortex sheet, or equivalently in the outer layer of the doublet sheet corresponding to the physical boundary layer. As mentioned above, the strength density of the equivalent vortex sheet  $\gamma$  is related to the strength of the vortex doublet sheet  $\mu$  as:

$$\gamma = \frac{\partial \mu}{\partial s} \quad \rightarrow \quad \mu(s) - \mu_o = \int_{s_o}^s \gamma ds, \quad (3)$$

where  $s$  is a coordinate tangent to the surface and  $\mu_o = \mu(s_o)$  is the value at a reference point  $s_o$ . We use the two different symbols  $\Gamma$  and  $\mu$  as a way to distinguish the two different representations of the surface as a vortex sheet and as a vortex doublet sheet. In other words,  $\mu$  is still the difference in potential across the surface.

Let the two wedge surfaces comprising a sharp edge be represented as vortex doublet sheets with strengths  $\mu^+(s^+)$  and  $\mu^-(s^-)$ , where the surface coordinates  $s^+$  and  $s^-$  define the sense of integration in (3) to be in the direction of the respective surface velocities. Figure 1 shows a qualitative example of this setup for a simple airfoil. The two vortex doublet sheets interact at the sharp edge where  $s = s_e$  and such that the remaining net sheet strength, say  $\Delta\mu_s = \mu^+(s_e^+) - \mu^-(s_e^-)$ , is related to the amount of circulation that must be released or shed into the fluid. The net doublet strength at the sharp edge is then ‘torn apart’ into vorticity and this can be interpreted as the mechanism of shedding. With regard to the method of images, consistency is achieved by recognizing that when the vortex doublet sheet is torn apart, one layer is shed into the fluid as a vortex sheet and the other layer goes into the object as the image sheet. The source of vorticity now appears naturally as a consequence of the vortex doublet sheet representing the physical boundary layer, as opposed to superimposing vorticity when the surface is described as a source-dipole distribution.

## 2.1 Example: Joukowski airfoils

To illustrate the above concepts, we apply them to a situation for which the potential flow is initially known, namely the impulsive motion to speed  $U$  of a Joukowski airfoil at angle of attack  $\alpha$ . The cusped trailing edge of these airfoils exhibits the ‘inverse square-root’ singularity due to the conformal mapping. For simplicity

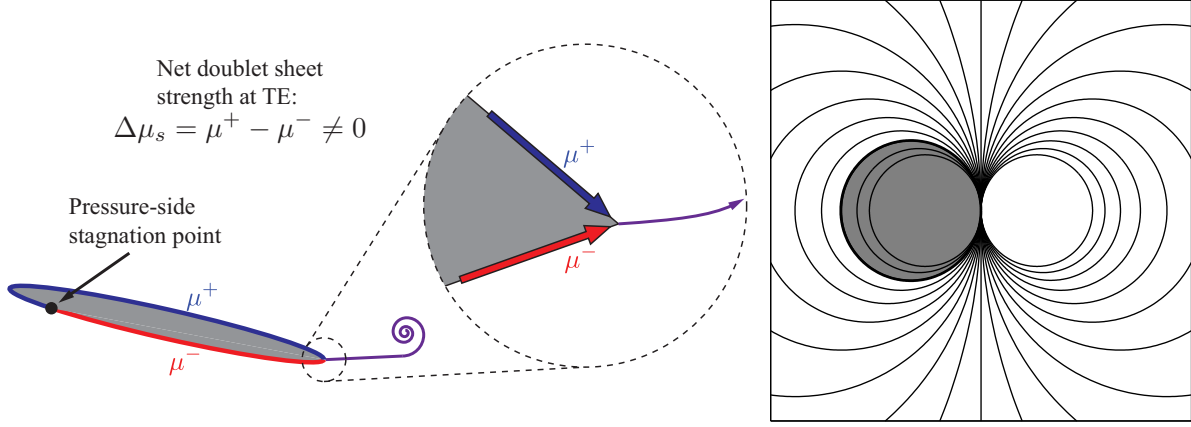


Figure 1: (*Left*) Example of trailing-edge shedding from an airfoil. The vortex doublet sheet strengths  $\mu^+$  and  $\mu^-$  represent the circulation in the boundary layers relative to the pressure-side stagnation point. It is assumed there is no leading-edge shedding. The net sheet strength at the trailing edge,  $\Delta\mu_s = \mu^+ - \mu^-$ , relates to the amount of circulation to be shed from the airfoil. (*Right*) Streamlines of a point vortex doublet. The shaded cylinder represents the solid surface in the virtual plane; the doublet location corresponds to the sharp edge in the physical plane.

of the expressions for the mapping, consider the flat-plate airfoil for which the mapping derivative on the surface of the plate goes as  $f' = d\zeta/dz \propto (1/\sin\nu)$ , where  $\nu$  is the angular coordinate in the virtual circle plane with  $\nu = 0$  corresponding to the trailing edge. The circle radius  $a$  is related to the plate chord as  $c = 2a$ . The velocity on the plate can be written as  $u = -u_\nu/\sin\nu$ , where  $u_\nu$  is the surface velocity in the circle plane. Hence, not only do we see why the Kutta condition is interpreted as  $u_\nu \rightarrow 0$  when  $\nu \rightarrow 0$ , but also that  $u_\nu \propto \sin\nu \propto 1/f'$ . Since we cannot evaluate the flow  $u$  in the physical plane when the Kutta condition is not satisfied, the device of a point vortex in the circle plane allows us to determine how  $u_\nu(0)$  can be made a stagnation point to regularize  $u(0)$ . The actual flow induced by the point vortex is somewhat superfluous, but its global effect on the flow, that is the induced circulation  $\Gamma$ , is the quantity of importance.

Now, since the flow cannot turn around the sharp edge, then after the impulsive motion, that is at  $t = 0^+$  and before any vorticity is shed, the flow will instantaneously appear as the steady potential flow around the airfoil with the proper circulation that satisfies the Kutta condition. We know there is a pressure-side stagnation point at  $\nu = \nu_o$ , which is chosen as the reference point (recall figure 1) for the calculation of  $\mu^+$  and  $\mu^-$  as:

$$\mu^\pm(\nu^\pm) - \mu_o = \int_{\nu_o}^{\nu^\pm} u_\nu a d\nu = Ua [\cos(\alpha - \nu) - \nu \sin \alpha]_{\nu_o}^{\nu^\pm}.$$

However, this state of affairs is not sustainable for  $t > 0^+$  and vorticity must be shed. To obtain the net strength at the trailing edge we take  $\nu^+ = 0$  and  $\nu^- = 2\pi$  so that  $\Delta\mu_s = \mu^+(0) - \mu^-(2\pi) = \pi U c \sin \alpha$ , where again  $c$  is the chord of the plate. Also note that the reference value  $\mu_o = \mu(\nu_o)$  cancels out. This  $\Delta\mu_s$  will be recognized as the steady-state bound circulation value of the airfoil. Hence, if the flow is to immediately reach the steady state at  $t > 0^+$ , then the airfoil must shed all of this circulation instantaneously into the starting vortex. The more realistic picture is that the airfoil gradually sheds this circulation over time and the bound circulation builds up, a phenomenon known as the Wagner effect [42]. In this regard, once some vorticity/circulation is shed into the fluid the flow field is altered so that the vortex doublet sheet strengths  $\mu^\pm$  also change to satisfy the no through-flow condition and the above equations can be recalculated from this new flow. This, along with movement of the pressure side stagnation point, will effect  $\Delta\mu_s$  and thus represent instant communication of flow changes to the trailing edge where shedding occurs.

### 3 Inviscid separation: tearing apart the doublet sheet

In the previous section we described separation as the vortex doublet sheet at the sharp edge being torn apart with one layer entering the fluid as the vortex sheet and the other layer entering the object as the image sheet. In order to accomplish this we must evaluate the flow at the edge to determine the rate of shed circulation. The main issue with modeling inviscid separation is, simply stated, the non-analyticity of the velocity field at the sharp edge, which prevents direct evaluation of the velocities  $u_-$  and  $u_+$  in (2) to calculate the rate of shed circulation. Even if the Kutta condition is satisfied at some instant, the problematic situation returns for any incremental change in the flow meaning that the velocities at the edge again become infinite. For the same reason, we cannot directly evaluate the vortex doublet sheet strengths  $\mu^+$  and  $\mu^-$  approaching the edge to determine  $\Delta\mu_s$  and thus enforce the Kutta condition to regularize the flow through the shedding of circulation. Therefore, just as in the example of §2.1, we require some device whose global characteristic allows us to affect a regular flow at the edge. Here, this device is provided by the *point vortex doublet* with strength  $\lambda \in \mathbb{C}$ .

The strength of a point vortex doublet  $\lambda$  differs from the strength of the vortex doublet sheet  $\mu$  in the same way that the strength of a point vortex  $\Gamma$  differs from the strength density of a vortex sheet  $\gamma$ . In fact, this concept is quite common in the formulation of vortex sheet roll-up problems, where  $\gamma$  may be infinite, for example at the free tip of a finite sheet, and is replaced by  $d\Gamma = \gamma ds$ , which remains locally finite. In the case of unsteady shedding at the sharp edge, not only are the velocities discontinuous they are also infinite, which technically leads to infinite circulations meaning that the net doublet sheet strength  $\Delta\mu_s = \mu^+ - \mu^-$  is not well defined. However, we can write  $d\lambda = \Delta\mu_s ds$  and interpret the point vortex doublet strength at the edge to be defined as:

$$\lambda = \lim_{\epsilon \rightarrow 0} \left[ \int_{-\epsilon}^{\epsilon} \Delta\mu_s ds \right], \quad (4)$$

where  $\epsilon$  is a vanishingly small arclength segment encompassing the sharp edge and  $\lambda$  is, in some sense, the ‘residue’ of the interaction of the two flows approaching the edge.

Now consider a point vortex doublet at the location of the sharp edge. We note that the streamlines of a vortex doublet are circles, which motivates us to look at the doublet in the circle plane located at  $\zeta_o$  (see figure 1). Note, however, that the only assumption we are making about the mapping to the physical plane is that it can take a portion of the circle to the local surface shape and has a singularity at the sharp edge. We will see in §5 that the mapping to a circular body is of no consequence on the geometry in the physical plane also being a doubly-connected region or not. The complex potential of this doublet is:

$$w_\lambda = -\frac{\lambda}{2\pi i} \frac{1}{\zeta - \zeta_o}. \quad (5)$$

In order to satisfy the no through-flow condition, then the streamline circle must coincide with the cylinder. This sets the orientation of the doublet, given by  $\arg(\lambda)$ , to be normal to the surface, which is obviously consistent with the vortex doublet sheet. Letting  $\zeta = \rho e^{i\nu}$  and  $\zeta_o = a$ , the flow induced by the doublet is tangential to the cylinder of radius  $a$  and is given by:

$$u_{\nu,\lambda} = -\frac{\lambda/a}{2\pi} \left( \frac{1}{2a(1 - \cos \nu)} \right) \equiv \frac{\Gamma_\lambda}{2\pi r(\nu)}. \quad (6)$$

The right-hand equation shows that the flow is similar to that induced by a point vortex with circulation  $\Gamma_\lambda = -\lambda/a$ , but which instead has a varying velocity along the streamline circle. As with the example in §2.1, the local distribution of this flow is again superfluous and we are concerned with its global characteristic, namely its strength  $\lambda$ , that will regularize the flow at the sharp edge. The relation between  $\Gamma_\lambda$  and  $\lambda$  suggested in (6) can also be obtained through integration of the above expression around the cylinder to yield the circulation  $\Gamma_\lambda = \Delta\mu_s$ . Some care is required in evaluating this singular integral (see Appendix A), but the result is:

$$\Gamma_\lambda = \oint_{|\zeta|=a} u_{\nu,\lambda} d\zeta = -\frac{\lambda}{a}. \quad (7)$$

Hence, the *integrated effect* of the doublet can again be interpreted as an equivalent bound circulation  $\Gamma_\lambda$  at the origin of the cylinder. However, the difference in the present case is that this circulation appears

naturally as a consequence of the interaction of the vortex doublet sheets at the sharp edge. Therefore, the requirement of a bounded velocity at the edge yields:

$$\left. \frac{dw_o}{d\zeta} \right|_{\zeta=\zeta_o} + \frac{\lambda}{(2\pi a^2)i} = \left. \frac{dw_o}{d\zeta} \right|_{\zeta=\zeta_o} - \frac{\Gamma_\lambda}{(2\pi a)i} = 0, \quad (8)$$

where  $dw_o/d\zeta$  is now the complex velocity in the virtual plane due to all other agencies except the doublet. However, it is important to notice that we do not actually construct a complex potential with the doublet at the sharp edge. Rather, this hypothetical potential and the fictitious flow  $u_{\nu,\lambda}$  determine an equivalent circulation that corresponds to the formation of vorticity to be shed from the sharp edge. In §4 the physics of how and why this occurs will be discussed with more mathematical rigor.

### 3.1 Consistency with steady aerodynamics

Equation (8) is quite interesting as it is exactly the same as the steady Kutta condition in classical aerodynamics. Here, we can consider  $\Gamma_\lambda$  as the starting vortex that is about to be shed from the trailing edge of the airfoil (if all circulation is shed instantly) after an impulsive motion to speed  $U$ . The velocity on the cylinder is:

$$u_\rho - iu_\nu = e^{i\nu} \left. \frac{dw_o}{d\zeta} \right|_{\zeta=ae^{i\nu}} = 0 - i[U \sin(\alpha - \nu)].$$

Substituting this into (8) and evaluating at the trailing edge  $\nu = 0$  gives:

$$|\Gamma_\lambda| = \left| \frac{\lambda}{a} \right| = 2\pi a U \sin \alpha \quad \rightarrow \quad C_L = \frac{\rho U |\Gamma_\lambda|}{\frac{1}{2}\rho U^2 c} = 2\pi \sin \alpha,$$

where  $c$  is the chord of the plate and recall that  $2a = c$ . Another way to interpret this is that as the starting vortex is shed and convects downstream to infinity, then its image approaches the origin to become the familiar bound circulation.

## 4 Inviscid vorticity generation and the unsteady Kutta condition

The unsteady Kutta condition has been notoriously obfuscated through the seeming fecundity of how it may be stated and the associated physical consequences, with its validity even being called into question. The review by [9] discusses this in part and also offers an extensive presentation of the viscous treatment of the Kutta condition through ‘triple-deck’ theory. Here, we are strictly focused on purely inviscid fluids governed by the Euler equation, which when prescribed to a potential flow has no inherent mechanism by which vorticity enters the fluid domain. Nonetheless, the basic physical implication of the Kutta condition is that the flow should remain bounded, namely an absence of singularities. This requirement then eventually leads to the determination of the amount of vorticity to be shed into the fluid.

Traditionally, the rate of shed circulation (for example (2)) is determined from Bernoulli’s equation, which in turn is obtained from an integration of the Euler equation. As such, Bernoulli’s equation represents the conservation of energy along certain trajectories, namely streamlines. Let the integration circuit be around the airfoil and with end points on the upper and lower sides of the trailing edge. With some rearranging, the result is:

$$\Delta p \equiv p^- - p^+ = -\rho \frac{d\Gamma_s}{dt} + \frac{1}{2}\rho u_-^2 - \frac{1}{2}\rho u_+^2, \quad (9)$$

where  $\Gamma_s = \phi^- - \phi^+$  with  $\phi^\pm$  being the harmonic potentials above and below the edge and with corresponding surface velocities  $u_\pm$  as before. Note that this form of Bernoulli’s equation requires the assumption of an incompressible flow. There has been much debate about whether or not a pressure jump should exist. [3], among many others, argue that there ought to be no infinities in the flow field and thus require  $\Delta p = 0$ . Recently, [1] examined the validity of the unsteady Kutta condition, which they interpreted as requiring a zero pressure jump at the trailing edge in addition to no flow singularities. They studied gust-airfoil interactions and calculated analytical solutions with and without the unsteady Kutta condition enforced,

which were then contrasted to numerical simulations in which the Kutta condition was neglected. They compared the far-field noise in each case and found that the numerics matched the analytic solution without an imposed Kutta condition. It was thus concluded that permitting an unsteady pressure jump at the edge results in an additional, yet unphysical noise term by scattering of the pressure singularity at the edge.

Requiring a zero pressure jump at the sharp edge is indeed physically grounded and, moreover, agrees with the dynamical consideration that free vortex sheets cannot support a pressure jump, a result that ought to remain congruent as the shedding edge is approached. However, enforcing this condition at the level of Bernoulli's equation glosses over the physics of the actual vorticity generation. In other words, while the Bernoulli equation may be used to obtain the rate of circulation put into the vortex sheet, it does not offer any insight on the mechanism of vorticity generation beyond the presence of a velocity discontinuity at the edge that forms the vortex sheet. To this end, consider the inviscid flow in which the Kutta condition is not yet satisfied at the sharp edge. Accordingly, the flow will navigate around the edge with infinite velocities driven by infinite pressures across the edge. Now recall the flow induced by the point vortex doublet discussed in §3. From (6) we see that  $u_{\nu,\lambda}$  is infinite, but continuous upon passing through the doublet, that is  $\nu > 0$  to  $\nu < 0$ . However, from (5) the harmonic potential  $\phi_\lambda = \text{Re}(w_\lambda) = -au_{\nu,\lambda} \sin \nu$  is infinite and discontinuous. Hence, remaining at the level of the Bernoulli equation, the doublet is associated with an unquantifiably infinite rate of circulation (and vorticity), even if  $\Delta p$  is made zero.

To rectify this peculiarity, we must return to the governing Euler equation. Since we are still within the framework of potential flow, we decompose the velocity field into two parts such that  $\mathbf{u} = \mathbf{u}_o + \mathbf{u}_\lambda = \nabla\phi_o + \nabla\phi_\lambda$ , where  $\phi_o$  is the potential due to all other effects besides the vortex doublet with potential  $\phi_\lambda$ . Then we can write the Euler equation as:

$$\left(\frac{\partial \mathbf{u}_\lambda}{\partial t} + \frac{1}{\rho} \nabla p\right) - \mathbf{u} \times \boldsymbol{\omega} = -\nabla \left(\frac{\partial \phi_o}{\partial t} + \frac{1}{2} q^2\right) \quad (10)$$

where  $q^2 = \mathbf{u} \cdot \mathbf{u}$  and  $\mathbf{u} \times \boldsymbol{\omega}$  is the Lamb vector, which is sometimes also termed the ‘vortex force’ [39]. Without the Kutta condition satisfied at the sharp edge, the pressure and so its gradient are both singular. Therefore, we see that the vortex-doublet-induced flow  $\mathbf{u}_\lambda$  must be such that this singularity is removed. In essence, the two terms in parentheses on the left-hand-side of (10) neutralize each other as a consequence of enforcing the Kutta condition so that no infinities appear in the flow. To see how this relates to the generation of vorticity, consider the curl of (10) to obtain the (two-dimensional) vorticity equation:

$$\frac{D\boldsymbol{\omega}}{Dt} = \nabla \times \left(-\frac{1}{\rho} \nabla p\right) = -\frac{1}{\rho} \nabla \times \nabla p + \frac{1}{\rho^2} \nabla \rho \times \nabla p. \quad (11)$$

Since the sharp edge is a non-analytic point where the pressure is singular, then the quantity  $\nabla \times \nabla p$  is not necessarily zero as this would require that  $p$  is  $C^2$  at this irregular point [17, chapter 16.6], which is often implicitly assumed. Even if  $p$  is twice continuously differentiable, we see that compressibility effects may be relevant (while being confined to the single point at the edge). Nonetheless, the result of neutralizing the infinite pressure gradient with the vortex doublet flow is the inviscid generation of vorticity. This pressure gradient is then the physical mechanism that rips apart the doublet to generate the shed vortex sheet as was more qualitatively discussed in §2. In fact, Batchelor (pg. 108) hints at this connection saying “... the ‘doublet’ motion far from the body which is set up by pressure gradients in the fluid...” in reference to the total linear momentum. Recall that in §3 we referred to the actual flow induced by the doublet as fictitious and that the global quantity of the doublet strength  $\lambda$  was of importance. This is because the flow is never actually established since it is simultaneously neutralized by the pressure gradient by virtue of the Kutta condition. Qualitatively, the flow turning around the sharp edge with infinite velocity is exactly opposed by the infinite velocity of the doublet at the edge.

The argument that the singular pressure gradient is neutralized by tearing apart the doublet can be made more rigorous by considering that a large pressure gradient may be interpreted as an impulse delivered to the fluid. Following [4] (chapter 6.10), the acceleration due to the singular pressure at the sharp edge results in the approximate governing equation

$$\frac{\partial \mathbf{u}}{\partial t} = -\frac{1}{\rho} \nabla p, \quad (12)$$

where these terms dominate and are very large for an infinitesimal amount of time corresponding to the enforcement of the Kutta condition due to an incremental change in the flow. Let  $\mathbf{u}'$  be the flow field just

prior to regularization and  $\mathbf{u}''$  the flow just after. Then we have:

$$\mathbf{u}'' - \mathbf{u}' = -\frac{1}{\rho}\nabla\Pi, \quad \Pi = \int p dt, \quad (13)$$

where  $\Pi$  is the pressure impulse. Hence, upon writing  $\mathbf{u}' = \mathbf{u}'_o + \mathbf{u}'_\lambda$  we see that  $\mathbf{u}'' = \mathbf{u}''_o$  is a regularized flow due to the neutralization of the singular pressure gradient. Of course this process repeats again and again as the flow evolves continuously in time. Since the inviscid generation of vorticity satisfies Kelvin's circulation theorem, then we can write:

$$-\int \Pi \hat{\mathbf{n}} dS = -\int \rho(\phi' - \phi'') \hat{\mathbf{n}} dS, \quad (14)$$

where  $S$  is a vanishingly small area encompassing the sharp edge (with unit depth into the page) and  $\hat{\mathbf{n}}$  is the unit vector normal to the shedding vortex edge. Then  $\Pi$  represents the impulse required to change the flow from  $\mathbf{u}'$  to  $\mathbf{u}''$ , namely the impulse required to impose the Kutta condition. The sharp edge is an irregular point that essentially determines the character of the flow, which can be seen by considering the relationship between the concept of a velocity potential  $\phi$  and the total kinetic energy of the fluid. As such, the force impulse corresponds to an 'acceleration reaction' or added-mass-like force. This is the reason the unsteady Kutta condition has a significant effect on the far-field noise as discussed by [1] (and the references therein).

Having dealt with the pressure singularity on the level of the Euler equation (momentum) as opposed to the Bernoulli equation (energy) results in a major physical difference. In the latter, the implication is that there is no loading at the edge, whereas with the former we now see that there is indeed a force associated with the inviscid generation of vorticity. More specifically, noting that  $\phi_\lambda$  and thus  $\mathbf{u}_\lambda$  are proportional to  $(-\lambda)$ , then (12) shows that the time rate-of-change of the doublet strength is related to the force of inviscid separation. More generally, returning to the original Euler equation (10) and recognizing that this force exists only at the sharp edge we can write:

$$\begin{aligned} 0 &= \lim_{\delta A \rightarrow 0} \int \left[ \left( \frac{\partial \mathbf{u}_\lambda}{\partial t} + \frac{1}{\rho} \nabla p \right) - \mathbf{u} \times \boldsymbol{\omega} \right] dA \\ &\therefore \rho \frac{d\lambda}{dt} \propto \rho u_s \Gamma_\lambda, \end{aligned} \quad (15)$$

where  $\delta A$  is an infinitesimal in-plane area (technically it is a volume per-unit-depth). The vorticity generated during the regularization is infinite, but in the limit the Lamb vector becomes  $-\mathbf{u} \times (\boldsymbol{\omega} \delta A_e) \rightarrow u_s \Gamma_\lambda$ , with  $u_s$  again being the shedding velocity tangential to the vortex sheet and  $\Gamma_\lambda$  being the circulation established by the vortex doublet as it is torn apart. Note the resemblance with the Kutta-Joukowski lift formula, again showing that the rate-of-change of the doublet strength is intimately linked to force. The left-hand-side of (10) is then zero everywhere in the analytic *fluid* domain and it follows that by excluding the non-analytic point at the sharp edge in the sense of Cauchy's integral theorem, we can then integrate the right-hand-side of (10) to obtain the Bernoulli equation in the usual way to give the rate of shed circulation as in (9) with  $\Delta p = 0$ , and this is necessarily consistent with (2).

## 5 Shedding equations

Having thoroughly justified the vortex doublet as the generating mechanism of the shed vortex sheet, we are now ready to derive equations for the shedding angle and velocity, and determine the rate of shed circulation. To derive these equations, first write the shedding velocity as  $u_s e^{i\theta_s}$ , where again  $u_s$  is tangential to the vortex sheet. Let  $u_+^e$ ,  $u_-^e$  be the velocities on the upper and lower faces of the sharp edge just upstream of the edge point (figure 2). These flows merge, generating the vortex sheet in the process, and downstream of the edge the velocities on either side of the vortex sheet are  $u_+$  and  $u_-$  as before. Since the vortex sheet is a material line, then from mass conservation we see that  $u_+^e = u_+$ ,  $u_-^e = u_-$ . The unit vectors describing the flow along the upper and lower surfaces of the edge may be written  $e^{-i\pi\beta/2}$  and  $e^{i\pi\beta/2}$ , respectively, where

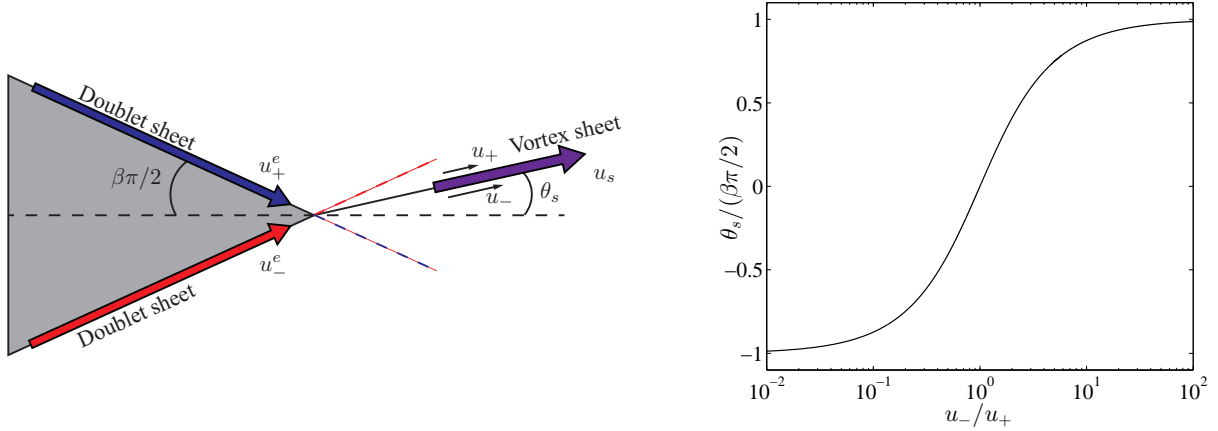


Figure 2: (*Left*) Schematic of the velocities near the shedding edge and forming into the shed vortex sheet. The vortex doublet sheets represent the solid surfaces and correspond to the circulation in the boundary layers. (*Right*) The shedding angle  $\theta_s$  as a function of the ratio of the velocities on the opposite sides of the shed vortex sheet  $u_-/u_+$  with  $\theta_s$  normalized by the interior edge semi-angle  $\beta\pi/2$ . There is a smooth variation between the tangential shedding limits of  $\pm\beta\pi/2$ .

the interior angle of the edge is  $\beta\pi$ . Therefore, that the vortex sheet is a material line gives the shedding angle as:

$$\theta_s = \arg \left( u_+ e^{-i\frac{\pi\beta}{2}} + u_- e^{i\frac{\pi\beta}{2}} \right) = \arctan \left( \frac{u_-/u_+ - 1}{u_-/u_+ + 1} \tan(\beta\pi/2) \right)$$

$$\frac{\theta_s}{\beta\pi/2} \approx \frac{4}{\pi} \arctan \left( \frac{u_-/u_+ - 1}{u_-/u_+ + 1} \right). \quad (16)$$

In fact, satisfying the above relation is equivalent to the mass and momentum conservation relations for a vortex sheet given by [45]. This is also equivalent to the shedding angle equation given by [47]; [they defined the wedge to be divided into two angles  $\Delta\theta_1$  and  $\Delta\theta_2$  that are relative to the vortex sheet, whereas here we define the shedding angle relative to the bisector angle; see their figure 4 and equation (5.4)]. The two relations are connected by the trigonometric identity  $\arctan(x) = \arccos(1/\sqrt{1+x^2})$ . Accordingly, this formula includes the two limits in the Giesing-Maskell model of  $\theta_s = \pm\beta\pi/2$ , and is also consistent with steady state flow where  $d\Gamma_s/dt = 0$  or  $u_+ = u_-$ . The approximate equation is exact for  $\beta = 0$ , and the error marginally increases for small, non-zero  $\beta$ , but quickly tends to zero for moderate angles and becomes exact again for  $\beta\pi = \pi/2$ . Figure 2 plots  $\theta_s/(\beta\pi/2)$  versus the ratio of the velocities on each side of the vortex sheet.

From (16) we see that the Giesing-Maskell model makes an implicit assumption that the flow is stagnated on one of the sides of the edge in order to give  $\theta_s = \pm\beta\pi/2$ . [3] adopt this model in their panel method numerics as do [32, 33] in their experimental investigations of the unsteady Kutta condition; each study considered oscillating airfoils characterized by a reduced frequency. In [15] this result can be traced back to an assumption made on the strength density  $\gamma$  of the shedding vortex sheet at the edge. Namely, in the physical plane  $\gamma$  is assumed constant, but in the transformed virtual plane it is made proportional to the inverse of the mapping singularity. It can be shown that if  $\gamma$  is non-zero at the end of the sheet the induced velocity there will be infinite. Hence, in the physical plane the induced velocity ought to be infinite, but in light §4 we can interpret this velocity as canceling the infinite velocity of the flow attempting to turn around the edge. The result is evidently a valid one, but corresponds to a special case. [36] arrived at a similar tangential shedding condition for the similarity solution of a vortex sheet shedding from the apex of a wedge. Namely, the sheet shape near the edge is assumed proportional to the similarity variable, which in turn is proportional to the circulation parameter of the sheet meaning an assumed constant strength density  $\gamma$ . The experiments of Poling & Telionis collectively identified a range of reduced frequencies  $k$  where the Giesing-Maskell model was applicable. Namely,  $k$  must be large enough so that as the foil oscillates the flow

on the leeward/suction edge face is comparatively stagnated. However, if  $k$  is too large, then it is possible that the flow turns around the edge, which is a result of both the real edge geometry never being perfectly sharp and the real fluid being viscous.

Now, to obtain the (complex conjugate) shedding velocity, we employ the mapping near a sharp edge of angle  $\beta\pi = \pi(2 - \frac{1}{n})$ , which is *locally* of the form [4]:

$$f' = \frac{nh(z)}{(z - z_o)^{1-n}} \quad \rightarrow \quad \zeta - \zeta_o = h_o(z - z_o)^n \quad \frac{1}{2} \leq n < 1, \quad (17)$$

for  $z$  very near  $z_o$  and where  $h_o = h(z_o)$  is non-zero and finite. In the event that a mapping of the entire geometry is known (Joukowski transform) we may use the full expression for  $h(z)$ ; see Appendix B. Due to the non-integer power on the  $(z - z_o)$  term in the mapping derivative we must proceed a bit differently. Let  $\Lambda \in \mathbb{C}$  be a complex length scale with  $|\Lambda| = K$  and  $\arg(\Lambda) = \theta_\Lambda$ , then write:

$$\begin{aligned} \frac{dw_o}{d\zeta} + \frac{\lambda}{(2\pi a)^2 i} &\approx 0 + \bar{\Lambda} \left( \frac{\zeta - \zeta_o}{K} \right)^{\frac{1}{n}-1} \frac{d^2 w_o}{d\zeta^2} = \bar{\Lambda} \left( \frac{h_o}{K} \right)^{\frac{1}{n}-1} (z - z_o)^{1-n} \frac{d^2 w_o}{d\zeta^2} \\ u_s e^{-i\theta_s} &= \lim_{\zeta \rightarrow \zeta_o} \left[ \left( \frac{dw_o}{d\zeta} + \frac{\lambda}{(2\pi a)^2 i} \right) f' \right] = nK \bar{\Lambda} \left( \frac{h_o}{K} \right)^{\frac{1}{n}} \frac{d^2 w_o}{d\zeta^2} \Big|_{\zeta=\zeta_o}. \end{aligned}$$

Note that the same result is arrived at if the circulation version of (8) were used instead. Dimensional consistency shows that the constant of proportionality in the mapping may be written as  $f_o K^{1-n}$  and consequently  $h_o/K = f_o/K^n$ . The choice of  $f_o$  is at our behest and simply specifies the rotational orientation of the edge relative to the coordinate system in the physical plane. Here,  $f_o = 1$  so that the  $\text{Re}(\zeta) > 0$  plane maps to the edge geometry as shown in figure 2. Since  $w_o$  was constructed as a complex potential, then we know that  $d^2 w_o/d\zeta^2 \in \mathbb{R}$  when  $\zeta = \zeta_o$ , which is a consequence of the no through-flow condition. Then  $\theta_\Lambda = \theta_s$  and the above becomes:

$$u_s = nK \frac{d^2 w_o}{d\zeta^2} \Big|_{\zeta=\zeta_o}. \quad (18)$$

The Kutta condition, which determines the rate of shed circulation, is obtained from the time derivative of (8):

$$\frac{d}{dt} \left( \frac{\Gamma_\lambda}{2\pi a i} \right) = \frac{d}{dt} \left( \frac{dw_o}{d\zeta} \right) = \left( \frac{d^2 w_o}{d\zeta^2} \frac{d\zeta}{dt} \right) \Big|_{\zeta=\zeta_o} = \frac{u_s}{nK} \frac{d\overline{w_o}}{d\zeta} \Big|_{\zeta=\zeta_o} = -\frac{u_s}{nK} \frac{\Gamma_\lambda}{2\pi a i}. \quad (19)$$

Hence, we see that the virtual circle radius  $a$  will cancel out and that the time rate-of-change of *shed* circulation  $\Gamma_s$  is:

$$\frac{d\Gamma_s}{dt} = u_s \left( \frac{\Gamma_\lambda}{nK} \right) \equiv u_s \gamma_s, \quad (20)$$

which is equivalent to (2). Note that  $\Gamma_\lambda/(nK) \equiv \gamma_s = u_- - u_+$  and  $u_s = \frac{1}{2}(u_+ + u_-) = (nK)d^2 w_o/d\zeta^2$  so that the  $(nK)$  factor cancels out of the expression for  $d\Gamma_s/dt$ . Lastly, we can rewrite the shedding angle as:

$$\theta_s = \arctan \left( \frac{\gamma_s}{2u_s} \tan(\beta\pi/2) \right) = \arctan \left( \frac{d\Gamma_s/dt}{2u_s^2} \tan(\beta\pi/2) \right). \quad (21)$$

These expressions are in terms of quantities obtained in a simulation and again the virtual cylinder radius  $a$  does not appear.

## 6 Example calculations

This section presents some example simulations to demonstrate the efficacy of the shedding equations derived in §5. Once the amount of vorticity to be shed is determined by these equations, we may describe it by or agglomerate it into a ‘vorticity element’ of our choice. Due to the simplistic implementation, we opt to use a point vortex method for this purpose.

## 6.1 Wagner problem

Consider only trailing-edge vortex shedding from a flat plate with chord  $c$  at  $\alpha = 15^\circ$  that is an impulsively accelerated to speed  $U$ . We use our regularized unsteady Kutta condition, namely (20), to place and convect constant strength trailing-edge vortices (TEVs);  $\gamma_s = \Gamma_\lambda/a$  is obtained from (8),  $u_s$  from (18). Since  $\beta = 0$ , then either (16) or (21) gives  $\theta_s \equiv 0$  for tangential shedding to the cusped edge. Non-dimensional time is  $t = Ut_d/c$  and is also equal to the number of chords traveled by the plate;  $t_d$  is dimensional time. The time-step is  $\Delta t = 0.02$ . The shedding equations of §5 are equivalent to those obtained in Appendix B where the Joukowski transformation is used directly. There, the length scale is  $K = c$  and  $n = 1/2$  so that  $nK = c/2 = a$ .

Figure 3(a) compares the shed circulation with Wagner’s circulation function [42, equation given by [25]]. The point vortex simulation under-predicts the Wagner function because the former accounts for the roll-up of the sheet, which slows the rate of shed circulation by reducing the velocity difference at the trailing edge. As such, the small-time behavior is when the two differ most. The inset plots the functions for  $0 \leq t \leq 0.2$ ; the simulation data were repeated with  $\Delta t = 0.002$  and  $0.0002$  to show convergence of the method. The difference of simulations with different  $\Delta t$  values is exacerbated at small time, but becomes much less with larger  $t$ . Figure 3(b) plots the same functions along with experimental measurement of trailing-edge circulation from [31]. They state there is a delay in circulation build-up because in their experiments the wing accelerates over a distance of 0.25 chords. From  $0.5 < t < 1.5$  the experimental data appear to agree better with the current simulation, again because the roll-up dynamics are accounted for here.

Most noteworthy is that at  $t = 0$  the simulations have a *finite* rate of shed circulation generation,  $d\Gamma_s/dt < \infty$ , whereas the Wagner function has an infinite slope. The (dimensional) lift  $L_y$  is computed from the equation [46]:

$$L_x - iL_y = -i\rho \left[ -2a \frac{d}{dt} (-\Gamma_\lambda) + \sum \Gamma_s \frac{d}{dt} \left( \bar{\zeta}_s - \frac{a^2}{\zeta_s} \right) \right], \quad (22)$$

where the first term represents the rate-of-change of the circulation at the origin,  $-\Gamma_\lambda$ , which is communicated to infinity instantaneously (see Appendix B) and the second term represents the contribution due to convection of the shed TEVs. We note that most point vortex models axiomatically set the circulation at the origin to zero in order to satisfy Kelvin’s circulation theorem at infinity, however, as mentioned by [46] this is technically incorrect if ‘vortex variation’ is considered. Inclusion of this term here represents the force associated with the inviscid generation of the vorticity. As discussed in §4 this an added-mass-like force, which is also communicated to infinity instantaneously via a change in the total kinetic energy of the fluid [4]. The  $d\Gamma_\lambda/dt$  term is large, but *finite* at  $t = 0$  (see figure 4 in §5 for more discussion), while the force from the TEVs is zero. In other words, a circulation is instantaneously established *round the airfoil*, but no circulation is shed into the fluid yet at  $t = 0^+$ . Figure 3(c) plots the lift coefficient from the experiments of [31], the Wagner lift function, which has a non-zero, finite lift at  $t = 0$ , and our simulation for the total lift as well as just the TEV contributions. At  $\alpha = 15^\circ$  there is sure to be leading-edge shedding, however there is decent agreement with our simulation and the experimental measurement. This is because after the acceleration phase the flow behind the plate then impinges on the suction side creating a tangential flow toward the leading edge [12] that detaches the LEV, thus leaving the TEV contributions. In fact, this impinging flow is a consequence of the non-zero (albeit, quickly decaying)  $d\Gamma_\lambda/dt$  term for  $t > 0$  when the plate is no longer accelerating. In essence, this represents added mass recovery and suggests that a particular subsequent maneuvering of the plate could further increase the recovery of the added mass initially ‘stored’ at infinity.

Figure 3(d) plots the point vortex locations at time  $t = 0.1$  from the simulations with  $\Delta t = 0.02$  and  $2 \times 10^{-4}$ , where 5 and 500 point vortices, respectively, have been shed to represent the vortex sheet. Lastly, figure 3(e) shows the initial roll up at  $t = 0.01$  for the  $\Delta t = 2 \times 10^{-4}$  case and further decreasing  $\Delta t$  supports the similarity of the roll-up process at small time.

## 6.2 The force of inviscid vorticity generation

In §4 it was shown that the time derivative of the doublet strength at the sharp edge corresponds to a force associated with the vorticity generation there; see (15). The simple relation between  $\lambda$  and  $\Gamma_\lambda$  (recall (7)),

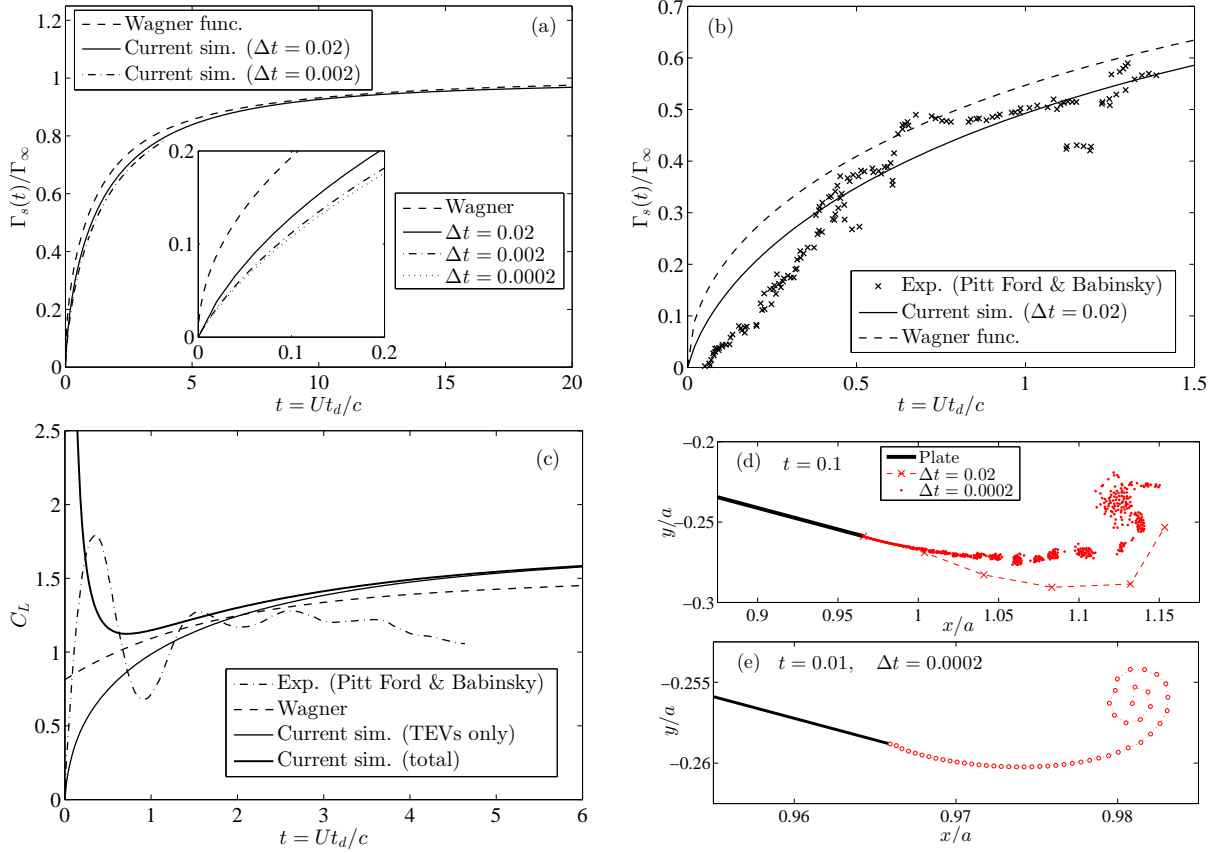


Figure 3: (a) The Wagner circulation function and the amount of normalized circulation shed from the trailing edge of a flat plate at  $\alpha = 15^\circ$  as obtained from a simulation with the shedding mechanism described in this paper with  $\Delta t = 0.02$  and  $0.002$ . Roll-up occurs in the simulations. (Inset) Small-time shed circulation showing convergence. (b) Comparison with experiment for  $\alpha = 15^\circ$  and  $Re = 30,000$ ; data adapted from [31]. (c) Lift coefficient from the same experiment, the Wagner lift, and the current simulation. (d) Point vortex locations for two simulations with different resolutions at time  $t = 0.1$ . For  $\Delta t = 0.02$  only 5 vortices have shed, whereas 500 vortices have shed for  $\Delta t = 2 \times 10^{-4}$ ;  $a = c/2$  is the half-chord length. (e) The initial vortex sheet roll-up at time  $t = 0.01$ .

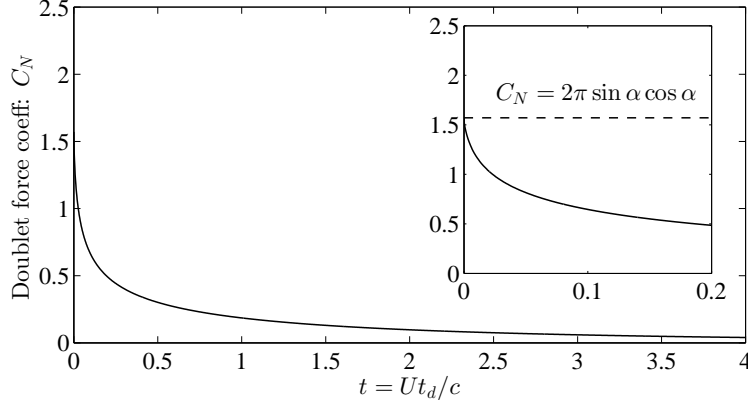


Figure 4: The vortex doublet normal force coefficient  $C_N$  due to shedding from the flat-plate airfoil in §6.1. At  $t = 0$  when there is an impulsive acceleration, this force represents a finite acceleration reaction force of magnitude  $C_N = 2\pi \sin \alpha \cos \alpha = \pi/2$  for  $\alpha = 15^\circ$  as shown by the dashed line in the inset plot. Each simulation limits to this theoretical value regardless of  $\Delta t$ .

allows this to be expressed in several ways:

$$\rho a \frac{d\Gamma_s}{dt} = \rho a u_s \gamma_s = \rho u_s \Gamma_\lambda = \rho \frac{d\lambda}{dt}. \quad (23)$$

With  $u_s$  being tangential to the vortex sheet and  $\Gamma_\lambda$  out-of-plane, the force is normal to the shed vortex sheet as mentioned in §4. This results from the fact that this term is related to the Lamb vector  $\mathbf{u} \times \boldsymbol{\omega}$  or the vortex force. Also, note that the density appears ‘naturally’ in the vortex doublet version since it is obtained from the Euler equation (recall 15) and accounts for the force at the sharp edge.

As an example, consider the flat-plate airfoil in §6.1. The doublet force is normal to the chord and is plotted in figure 4. At  $t = 0$  when there is an impulsive acceleration to speed  $U$ , this force is *finite* and corresponds to an added-mass-like force, say  $N$ . This is easy to show from the attached potential flow at  $t = 0$  where  $u_s(0) = U \cos \alpha$  and  $|\Gamma_\lambda(0)| = \pi c U \sin \alpha$  so that  $N(0) = \rho d\lambda/dt = \pi \rho c U^2 \sin \alpha \cos \alpha \rightarrow C_N = 2\pi \sin \alpha \cos \alpha$ . In other words, the infinitesimal length of the vortex sheet closest to the trailing edge can be thought of as part of the airfoil surface. Much like the caudal fin of a fish, this vortex sheet accelerates fluid by preventing flow around the sharp edge even in the case of a cusped edge where the shedding angle is always tangential.

### 6.3 Starting flow past an infinite wedge

Now we perform an inviscid simulation that employs the shedding equations of §5 for the case of a non-cusped edge. For this purpose we simulate the starting flow past an infinite wedge of interior angle  $\beta\pi$ . The attached potential flow in the physical plane is described by  $w = -iat^m z^n$  with  $\zeta = z^n$  so that the upwards uniform flow  $at^m$  in the virtual plane maps to the wedge geometry as shown in figure 2.

For comparison we use the similarity solutions of [36]. As stated by [14] a system of point vortices cannot continually and accurately represent the detailed sheet structure. Therefore, the relation given by Pullin for the amount of circulation shed and its time-derivative provide better metrics for comparison:

$$\Gamma_s(t) = J C^n L^2/t, \quad (24)$$

where  $L(t) = a^{1/(2-n)} t^{(1+m)/(2-n)}$  is a time-dependent length scale used to non-dimensionalize the spatial coordinates with  $L' = CL$  with  $C = [(2-n)(1-n)/(1+m)]^{1/(2-n)}$ . [48] also uses  $L$  in viscous Navier-Stokes simulations where the associated scale Reynolds number is  $Re_s(t) = (L^2/t)/\nu$ ; the values  $m = 0$ ,  $a = 1$  and  $\nu = 0.002$  were used in her study. In the current paper we also choose  $a = 1$  and conform to the spatial scalings  $L$  and  $L'$  where appropriate.

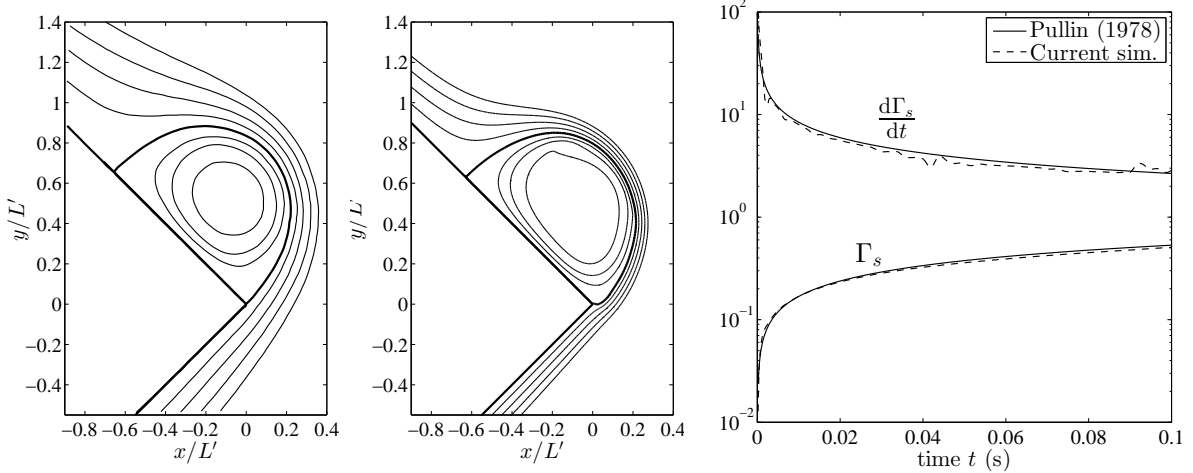


Figure 5: Comparison of results for the case of  $\beta\pi = \pi/2$  and  $m = 0$ . Streamlines (*left*) adapted from [36] and (*middle*) the point vortex simulation at  $t = 0.1$  s of the current paper with  $\Delta = 2 \times 10^{-4}$  s and total run time  $t_f = 0.1$  s; the streamfunction values are the same as Pullin with the bold line as  $\psi/(L'a) = 0$ . (*Right*) the amount and rate of shed circulation:  $\Gamma_s(t)$  and  $d\Gamma_s/dt$ .

At the initial instant  $t = 0$  the flow due to the ‘other agencies’ consists only of the uniform flow  $dw_o/d\zeta = at^m$  so that (18) gives  $u_s = nd^2w_o/d\zeta^2 = 0$  and cannot be used. However (21), which stems from an application of mass conservation, can be used with the assumption that at the onset of motion the flow on the leeward side ( $u_+$ ) is stagnated compared to the windward side ( $u_-$ ). Hence,  $u_-/u_+ \rightarrow +\infty$  and consequently  $\theta_s(0) = \beta\pi/2$  meaning that the flow *initially* separates tangentially to the windward wedge face. Using this result gives the initial condition  $u_s(0) = \gamma_s(0)/2$ . Both [38] and [36] state that the flow separates tangentially *for all time* (as does the Giesing-Maskell model). In Rott’s case this is due to the use of the single-vortex Brown-Michael model, while in Pullin’s case it is related to the similarity solution whose governing equation does not explicitly contain time. In a truly unsteady flow it is clear that as the vortex sheet rolls up, then the flow on the leeward wedge face will not be stagnated for  $t > 0$  and thus the flow may separate at an arbitrary angle. This is explicitly confirmed by [48].

Figure 5 shows the comparison of Pullin’s calculations with the results of our simulation for the case of  $\beta\pi = \pi/2$  ( $= 90^\circ$ ) and  $m = 0$ . The simulations were computed with  $\Delta t = 2 \times 10^{-4}$  s and a total run time of  $t_f = 0.1$  s. The simulation streamlines are at time  $t = t_f$  and unsurprisingly display some waviness, which again is due to local point vortex interactions, but there is decent agreement. More importantly, however, there is excellent agreement with the circulation/shedding rate, which validates the efficacy of the shedding equations derived in this paper.

## 7 Concluding remarks

It was shown that the inviscid generation mechanism of two-dimensional vortex sheets shed from sharp edges can be represented by a vortex doublet at the edge. The doublet itself appears as a result of representing the solid surface and its attached inviscid boundary layer by a vortex doublet sheet. This is different from the conventional source-dipole sheet, as the strength of the vortex doublet sheet is more naturally associated with the circulation in the boundary layer represented as a vortex sheet. Qualitatively, when the doublet sheet is ‘torn apart’ one layer corresponds to the shed vortex sheet and the other layer is the image sheet inside the surface. Equations for the shedding angle and velocity are derived and that are then used to determine the rate of shed circulation via the Kutta condition. The equation derived for the angle of the shedding vortex sheet stems from an application of mass conservation and is equivalent to that given by [47]. The limiting cases for which the flow is stagnated on one of the edge faces, as implicitly assumed in the Giesing-Maskell model, are included as well as the steady case where the flow leaves the edge along the

bisector angle. There is a smooth variation, with respect to the ratio of velocities at the edge, between each of these limiting cases. The assumption of stagnated flow used in other models leads to the incompatibility with the steady case and stems from an assumption made on the local vortex sheet strength at the edge.

The strength of the vortex doublet sheets correspond to the amount of circulation developed along the surfaces relative to a reference point. At the shedding edge, the net strength corresponds to the amount of circulation to be shed into the fluid. The Kutta condition is interpreted as the physical requirement that the flow remain bounded, that is without singularities. Similar to other studies, we conclude that this does not allow a pressure jump across the sharp edge. However, we consider this at the level of the Euler equation instead of Bernoulli's equation. It was argued that the infinite pressure and gradient, which would exist if the flow turned around the corner, is balanced by the infinite flow induced by the vortex doublet at the edge. The result of this interaction is the inviscid generation of vorticity, which is quantified as circulation that is put into the shedding vortex sheet. In other words, the large pressure gradient is the mechanism that tears apart the vortex doublet to generate vorticity and the two are immediately neutralized in the process so that there is no pressure jump across the shed vortex sheet. The time rate-of-change of the vortex doublet strength results in a force that corresponds to the vorticity generation and thus there is a loading on the edge.

In the case of a finite body (e.g. airfoil) the vortex doublet force communicates a circulation to infinity generating a force normal to the shed vortex sheet. When the body accelerates, even impulsively, this force is finite and thus represents a connection between the potential flow added mass concept and vortex shedding while avoiding the need for geometry-dependent coefficient expressions associated with the former. The non-zero value of this force even after the acceleration phase represents the recovery of added mass 'stored' at infinity. Having dealt with the generation and shedding of vorticity at the level of the Euler equation eliminates the need to distinguish among 'circulatory' and 'non-circulatory' forces. Demonstration of the shedding equations was shown with different test cases using a simple point vortex method with no other special techniques employed. The results compared favorably with existing theory, computation, and experiment.

The second part of this paper series presents the inviscid vortex sheet model of separation from a *smooth* surface where the separation point is not necessarily fixed by a geometric singularity as in the cases of cusped or sharp edges. Rather, the separation point is able to move relative to the surface and represents a topological singularity. In addition, the problem of predicting the location of the separation point is considered. The novelty of the proposed approach lies in the use of computationally inexpensive inviscid potential models of the flow to predict this viscous phenomenon.

## Acknowledgments

The authors wish to acknowledge the partial support of the AFOSR and ONR.

## Appendix A: Vortex doublet from point vortex shedding

In §3 a point vortex doublet at the sharp edge appeared as a result of the interaction of the vortex doublet sheets representing the two surfaces comprising the wedge. The shedding of vorticity was interpreted as the doublet being torn apart. In the continuous sense, the result is one half of the doublet shedding into the fluid as a vortex sheet, whereas the other half corresponds to the image sheet in the solid.

In the discrete sense, the vortex doublet is torn apart into two point vortices of equal and opposite strength. In fact, the authors' initial investigation of this problem began with this 'derivation' of the vortex doublet as a 'backwards time' limit of a point vortex  $\Gamma_o$  and its image approaching the shedding edge as shown in figure 6. With reference to this figure and writing  $\frac{1}{2}\delta\zeta = a[1 - \text{Re}(e^{i\epsilon})]$  then this doublet is 'created' from the limit:

$$\lambda \equiv \lim_{\delta\zeta \rightarrow 0} \Gamma_o \delta\zeta = \lim_{\epsilon \rightarrow 0} 2\Gamma_o a(1 - \cos \epsilon).$$

Next, we show how to evaluate the circulation integral (7) due to the vortex doublet flow around the cylinder

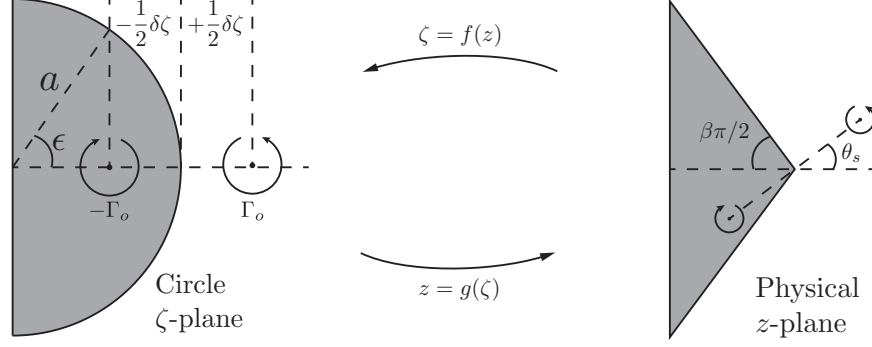


Figure 6: The circle and physical planes showing the limit of a vortex and its image approaching each other to define the vortex doublet of strength  $\lambda = \lim_{\delta\zeta \rightarrow 0} \Gamma_o \delta\zeta = \lim_{\epsilon \rightarrow 0} 2\Gamma_o a(1 - \cos \epsilon)$ . The angle  $\epsilon$  is exaggerated for clarity. The physical plane only shows the geometry near the sharp edge of interior angle  $\beta\pi$ . The shedding angle is  $\theta_s$ .

( $|\zeta| = a$ ). Substituting  $u_{\nu,\lambda}$  from (6) yields:

$$\Gamma_\lambda = \frac{-\lambda}{a} \lim_{\epsilon \rightarrow 0} \left[ \frac{1}{2\pi a} \int_{0+\epsilon}^{\pi-\epsilon} \frac{a d\nu}{2(1 - \cos \nu)} \right] = \frac{-\lambda}{a} \lim_{\epsilon \rightarrow 0} \left[ \frac{-1/4\pi}{\tan(\nu/2)} \Big|_\epsilon^{\pi-\epsilon} \right].$$

We have written the expression in this way so that the quantity in the square brackets may be considered as a dimensionless circumference-averaged velocity induced by the doublet. With the limit definition of  $\lambda$  from above, then we have:

$$\Gamma_\lambda = \frac{-1}{a} \lim_{\epsilon \rightarrow 0} \left[ \left( \frac{\Gamma_o a}{\pi} \right) \frac{1 - \cos \epsilon}{\tan(\epsilon/2)} \right] = \frac{-1}{a} \lim_{\epsilon \rightarrow 0} \left[ \frac{\Gamma_o a}{\pi} \epsilon + O(\epsilon^3) \right] = -\frac{\lambda}{a}.$$

Technically, this is a slightly different limit from  $\lambda = \lim_{\epsilon \rightarrow 0} (\Gamma_o a \epsilon^2 + O(\epsilon^4))$ . However, since any information about  $\Gamma_o$  remains unspecified, then we can simply require that  $\Gamma_o$  now increases as  $\epsilon^{-1}$  rather than  $\epsilon^{-2}$  and such that the same constant  $\lambda$  is yielded.

## Appendix B: Mapping ambiguities

This appendix essentially recapitulates the work of [10] that showed the cancelation of singularities via a mapping ambiguity for point vortex shedding from a flat plate. We then extend the same idea to arbitrarily angled edges. Point vortex models have seen varying degrees of success, but with time have been improved to provide accurate results. One fundamental issue with these methods is the proper introduction of new vorticity to satisfy the unsteady Kutta condition. The equations of motion are singular at the initialization of a vortex at a sharp edge.

Let  $w$  be the complex potential,  $z$  and  $\zeta$  be the complex variables in the physical and virtual planes, respectively, and  $f(z) = \zeta$  be the mapping between the planes. Now consider a point vortex of circulation  $\Gamma_k$  at a location  $z_k$  that is close to the shedding edge at  $z_o$ . Taking into account the Routh correction in the Kirchhoff velocity, then requiring that the flow remain bounded yields:

$$\begin{aligned} & \lim_{z_k \rightarrow z_o} \left| \left( \frac{dw}{dz} - \frac{\Gamma_k}{2\pi i} \frac{1}{z - z_k} \right)_{z=z_k} \right| \\ &= \lim_{\zeta_k \rightarrow \zeta_o} \left| \left\{ \left( \frac{dw_o}{d\zeta} - \frac{\Gamma_k}{2\pi i} \frac{1}{\zeta - \zeta_k^i} + \frac{\Gamma_k}{2\pi i} \frac{f''}{2(f')^2} \right) f' \right\}_{\zeta=\zeta_k} \right| < \infty, \end{aligned} \quad (25)$$

where  $dw_o/d\zeta$  is the complex velocity due to all other agencies beside the vortex *and* its inverse image at  $\zeta_k^i$ , which is the second term on the right-hand side, and the Routh correction is the third term. If there is

any hope of canceling these singularities, we must determine the limiting behavior and the *sign* of the Routh correction term.

First consider the Joukowski transformation for a flat-plate airfoil that maps a circle of radius  $a$  in the  $\zeta$ -plane to the slit  $-a \leq x \leq a$  on the real axis of the  $z$ -plane:

$$\zeta = z + (z^2 - a^2)^{\frac{1}{2}}, \quad z = \frac{1}{2} \left( \zeta + \frac{a^2}{\zeta} \right).$$

Note that  $a = c/2$  is the half-chord of the plate and we take  $z = \zeta = +a$  as the trailing edge and  $z = \zeta = -a$  as the leading edge. Using these relations, the term representing the Routh correction in terms of  $\zeta$  is:

$$\frac{f''}{2(f')^2} = -\frac{a^2}{\zeta(\zeta^2 - a^2)}.$$

Substituting and noting from the Milne-Thomson circle theorem that  $\zeta_k^i = a^2/\bar{\zeta}_k$ , then we obtain:

$$\lim_{\zeta_k \rightarrow \pm a} \left| \left( \frac{dw_o}{d\zeta} - \frac{\Gamma_k}{2\pi i} \left[ \frac{1}{\zeta_k - a^2/\bar{\zeta}_k} + \frac{a^2}{\zeta_k(\zeta_k^2 - a^2)} \right] \right) f' \right| < \infty, \quad (26)$$

and there is no approach of  $\zeta_k \rightarrow \pm a$  that will allow cancellation of the singularities (see Appendix C). The inversion of the Joukowski transformation to obtain  $\zeta = f(z)$  technically has two valid solutions. Normally the (+) sign is taken to map the domain outside the airfoil,  $D_z$ , to the domain outside the cylinder,  $D_\zeta$ . The (−) sign maps  $D_z$  to the *inside* of the cylinder. However, for a point on the boundary either transformation will map to the circle. Let the roots of the inverse map be  $f_+$  and  $f_-$ , then we further note that for the singularity points at  $z \rightarrow \pm a$  we have:

$$\begin{aligned} f_- \rightarrow f_+ = \pm a, \quad -(f'_-) \rightarrow f'_+ \rightarrow \pm\infty, \quad -(f''_-) \rightarrow f''_+ \rightarrow -\infty, \\ \therefore \frac{f''_-}{2(f'_-)^2} \rightarrow -\frac{f''_+}{2(f'_+)^2}, \end{aligned}$$

where the upper/lower signs (where applicable) are for the trailing/leading edges, respectively. At these particular singular points, the correctness of either map is ambiguous since the second and third equations both approach  $|\infty|$ .

Therefore, we may choose the mapping to be  $f_-$  in the limit of  $z_k \rightarrow \pm a$ , which changes the sign between the two terms in square brackets in (26). Letting  $\zeta_k = \rho_k e^{i\nu_k}$ , the limit of these terms is only finite for  $\nu_k = 0$  and  $\pi$ , so that shedding occurs tangentially from the edges. With the limit equaling  $\pm a^{-1}$  (see Appendix C) we then have:

$$\lim_{\zeta_k \rightarrow \pm a} \left| \left( \frac{dw_o}{d\zeta} \mp \frac{\Gamma_k}{2\pi ai} \right) f' \right| < \infty \quad \rightarrow \quad \therefore \frac{dw_o}{d\zeta} \Big|_{\zeta_k = \pm a} \mp \frac{\Gamma_e}{2\pi ai} = 0,$$

where the second equation is the fulfillment of a bounded velocity field and is equivalent to (8). Also, in taking the limit above we let  $\Gamma_k \rightarrow \Gamma_e$  to denote that  $\Gamma_e$  is an edge vortex currently residing on the airfoil.

The shedding velocity is obtained as in §5 where  $dw/d\zeta$  is expanded in a Taylor series. The rate of shed circulation is obtained similarly as a time derivative of the bounded velocity requirement equation. As a result we have:

$$u_s = \pm a \frac{d^2 w_o}{d\zeta^2} \Big|_{\zeta = \pm a}, \quad \frac{d\Gamma_s}{dt} = u_s \left( \pm \frac{\Gamma_e}{a} \right) \equiv u_s \gamma_s,$$

where  $|\gamma_s| = |\Gamma_e/a|$ . An important comment about the Kutta condition is in order. The image *system* of the vortex  $\Gamma_e$  includes a vortex of strength  $-\Gamma_e$  at the inverse location and a vortex of strength  $+\Gamma_e$  at the origin. The circulation  $+\Gamma_e$  at the origin is mapped to infinity by way of the Joukowski transform. An apparent violation of Kelvin's circulation theorem can be rectified by considering the times  $t_e^-$  and  $t_e^+$  just before and after the formation of  $\Gamma_e$ . The change from  $t_e^-$  to  $t_e^+$  requires that a *bound* circulation  $-\Gamma_e$  be established at the origin and, with the circulation  $+\Gamma_e$  at infinity, Kelvin's circulation theorem is then satisfied. In other words, the plate motion from  $t_e^-$  to  $t_e^+$  establishes a bound circulation and which is instantaneously communicated to infinity.

Hence, for the case of a flat plate obtained by the Joukowski transformation, we have implemented a regularized unsteady Kutta condition in an exact analytical form for an inviscid shedding method. The shedding velocity and rate of circulation at the edge are obtained. For a point vortex method, this allows placement of constant strength vortices  $\Delta\Gamma_s \approx u_s(\Gamma_e/a)\Delta t$  directly at the edge and which will shed with finite velocity  $u_s$ .

Next, consider the possibility of a similar singularity cancellation for edges of arbitrary angle. Recalling the mapping of the sharp edge in (17), we then have for the Routh term:

$$\frac{f''}{2(f')^2} = -\frac{(1-n)}{2n(\zeta - \zeta_o)}.$$

Without loss of generality, take  $z_o = \zeta_o = 0$  and recognizing that here  $\zeta_k^i = \bar{\zeta}_k$ , then the bounded flow requirement is:

$$\lim_{\zeta_k \rightarrow 0} \left| \left\{ \left( \frac{dw_o}{d\zeta} - \frac{\Gamma_k}{2\pi i} \left[ \frac{1}{\zeta_k - \bar{\zeta}_k} + \frac{(1-n)}{2n\zeta_k} \right] \right) f' \right\} \right| < \infty.$$

Upon separating the real and imaginary parts of the terms in square brackets, one will find that to keep the real part finite as  $\rho_k \rightarrow 0$  we must take  $\cos \nu_k = 0$ , meaning that  $\nu_k = \pm\pi/2$  and so  $\sin \nu_k = \pm 1$ . Then the imaginary part becomes  $\pm 1/(2n\rho_k)$ , and there is no value of  $\frac{1}{2} \leq n < 1$  to keep this finite as  $\rho_k \rightarrow 0$ . However, only for the cusped edge case of  $n = \frac{1}{2}$  can we apply the multi-valued mapping ambiguity as above. As such we have for the imaginary part:

$$\lim_{\rho_k \rightarrow 0} \left\{ \pm \left( \frac{1-2n}{2n\rho_k} \right) \Big|_{n=\frac{1}{2}} \right\} = \frac{1}{C},$$

where  $C$  is some length scale. Since  $\nu_k = \arg(\zeta_k) = \arg(z_k^n) = \theta_k/2$ , then in the physical plane this means that  $\theta_k = \pm\pi$ . Hence, the vortex again sheds tangentially from the cusped edge as expected. However, here no further information is obtained. It is now clear that the mapping ambiguity is only applicable to cusped edges when the mapping is actually multivalued.

## Appendix C

Here, we show the details of the limiting process discussed in Appendix A for the Joukowski transform:

$$\frac{1}{\zeta - a^2/\bar{\zeta}} \pm \frac{a^2}{\zeta(\zeta^2 - a^2)} = \frac{\bar{\zeta}}{\zeta\bar{\zeta} - a^2} \pm \frac{a^2\bar{\zeta}(\bar{\zeta}^2 - a^2)}{\zeta\bar{\zeta}(\zeta^2 - a^2)(\bar{\zeta}^2 - a^2)}.$$

We have dropped the subscript 'k' for convenience and the  $\pm$  corresponds to the mappings  $f_+$  and  $f_-$ , respectively. Letting  $\zeta = \rho e^{i\nu}$ , then after some rearranging we have:

$$\frac{\rho e^{-i\nu}}{a^2} \left[ \frac{1}{\frac{\rho^2}{a^2} - 1} \pm \frac{\frac{\rho^2}{a^2} e^{-i2\nu} - 1}{\frac{\rho^2}{a^2} \left( \frac{\rho^4}{a^4} + 1 - 2\frac{\rho^2}{a^2} \cos(2\nu) \right)} \right].$$

By inspection, if  $f_+$  is the mapping then there is no path which results in a finite limit for both the real and imaginary parts. However, if  $f_-$  is the mapping, then for  $\nu = 0$  and  $\pi$  the imaginary part is zero. Hence, shedding occurs tangentially to the plate as expected. The values  $\nu = 0$  and  $\pi$  correspond to the trailing and leading edges, respectively, so that the vortex advects outward from the plate. The real part of the above equation is:

$$\lim_{\rho \rightarrow a} \left\{ \frac{\pm \rho}{a^2} \left[ \frac{1}{\frac{\rho^2}{a^2} - 1} - \frac{\frac{\rho^2}{a^2} - 1}{\frac{\rho^2}{a^2} \left( \frac{\rho^4}{a^4} + 1 - 2\frac{\rho^2}{a^2} \right)} \right] \right\} = \frac{\pm 1}{a},$$

where the upper/lower signs now apply to the trailing/leading edges, respectively.

## References

- [1] AYTON, L. J., GILL, J. R. & PEAKE, N. 2016 The importance of the unsteady kutta condition when modelling gust-aerofoil interaction. *Journal of Sound and Vibration* **378**, 28–37.
- [2] BAKER, G. R., MEIRON, D. I. & ORSZAG, S. A. 1982 Generalized vortex methods for free-surface flow problems. *Journal of Fluid Mechanics* **123**, 477–501.
- [3] BASU, B. C. & HANCOCK, G. J. 1978 The unsteady motion a two-dimensional aerofoil in incompressible inviscid flow. *Journal of Fluid Mechanics* **87**, 159–178.
- [4] BATCHELOR, G. K. 1967 *An Introduction to Fluid Dynamics*. Cambridge, UK: Cambridge University Press.
- [5] CHORIN, A. J. & BERNARD, P. S. 1973 Discretization of a vortex sheet with an example of roll-up. *Journal of Computational Physics* **13**, 423–429.
- [6] CLEMENTS, R. R. 1973 An inviscid model of two-dimensional vortex shedding. *Journal of Fluid Mechanics* **57** (2), 321–336.
- [7] CONLISK, A. T. & ROCKWELL, D. 1981 Modeling of vortex-corner interaction using point vortices. *Physics of Fluids* **24**, 2133–2142.
- [8] CORTELEZZI, L. & LEONARD, A. 1993 Point vortex model of the unsteady separated flow past a semi-infinite plate with transverse motion. *Fluid Dynamics Research* **11**, 263–295.
- [9] CRIGHTON, D. G. 1985 The Kutta condition in unsteady flow. *Annual Review of Fluid Mechanics* **17**, 411–445.
- [10] DEVORIA, A. C. & MOHSENI, K. 2018 Desingularized trailing-edge shedding from a flat plate with a point vortex method. In *Proceedings of the AIAA Science and Technology Forum*, pp. 1–7. Kissimmee, FL, USA.
- [11] DEVORIA, A. C. & MOHSENI, K. 2018 Vortex sheet roll-up revisited. *Journal of Fluid Mechanics* In Review.
- [12] DEVORIA, A. C. & RINGUETTE, M. J. 2013 On the flow generated on the leeward face of a rotating flat plate. *Experiments in Fluids* **54** (4), 1–14.
- [13] EPPS, B. P. & ROESLER, B. T. 2018 Vortex sheet strength in the Sears, Küssner, Theodorsen, and Wagner aerodynamics problems. *AIAA Journal* Accepted for publication.
- [14] FINK, P. T. & SOH, W. K. 1974 Calculation of vortex sheets in unsteady flow and applications in ship hydrodynamics. In *Proceedings of the 10th Symposium on Naval Hydrodynamics*, pp. 463–489. Cambridge, MA, USA.
- [15] GIESING, J. P. 1969 Vorticity and Kutta condition for unsteady multienergy flows. *ASME Journal of Applied Mechanics* **36** (3), 608–613.
- [16] GRAHAM, J. M. R. 1983 The lift on an aerofoil in starting flow. *Journal of Fluid Mechanics* **133**, 413–425.
- [17] GREENBERG, M. D. 1998 *Advanced Engineering Mathematics*, 2nd edn. New Jersey: Prentice Hall.
- [18] HAROLDSSEN, D. J. & MEIRON, D. I. 1998 Numerical calculation of three-dimensional interfacial potential flows using the point vortex method. *SIAM Journal of Scientific Computing* **20** (2), 648–683.
- [19] JONES, M. A. 2003 The separated flow of an inviscid fluid around a moving flat plate. *Journal of Fluid Mechanics* **496**, 405–441.

- [20] KATZ, J. 1981 A discrete vortex method for the non-steady separated flow over an airfoil. *Journal of Fluid Mechanics* **102**, 315–328.
- [21] KELLOGG, O. D. 1929 *Foundations of Potential Theory*, 1st edn. Berlin: Springer.
- [22] KRASNY, R. 1986 Desingularization of periodic vortex sheet roll-up. *Journal of Computational Physics* **65** (2), 292–313.
- [23] KRASNY, R. 1987 Computation of vortex sheet roll-up in the Trefftz plane. *Journal of Fluid Mechanics* **184**, 123–155.
- [24] LEONARD, A. 1980 Vortex methods for flow simulation. *Journal of Computational Physics* **37** (3), 289–335.
- [25] LI, J. & WU, Z. 2015 Unsteady lift for the Wagner problem in the presence of additional leading/trailing edge vortices. *Journal of Fluid Mechanics* **769**, 182–217.
- [26] LIDTHILL, J. 1986 Fundamentals concerning wave loading on offshore structures. *Journal of Fluid Mechanics* **173**, 667–681.
- [27] MASKELL, E. C. 1971 On the Kutta-Joukowski condition in two-dimensional unsteady flow. *Unpublished note, Royal Aircraft Establishment, Farnborough, England*.
- [28] MICHELIN, S. & LLEWELLYN SMITH, S. G. 2009 An unsteady point vortex method for coupled fluid-solid problems. *Theoretical and Computational Fluid Dynamics* **23** (2), 127–153.
- [29] MUSKHELISHVILI, N. I. 1946 *Singular Integral Equations*, 1st edn. Moscow: P. Noordhoff Ltd.
- [30] NITSCHKE, M. & KRASNY, R. 1994 A numerical study of vortex ring formation at the edge of a circular tube. *Journal of Fluid Mechanics* **276**, 139–161.
- [31] PITT FORD, C. W. & BABINSKY, H. 2013 Lift and the leading-edge vortex. *Journal of Fluid Mechanics* **720**, 280–313.
- [32] POLING, D. R. & TELIONIS, D. P. 1986 The response of airfoils to periodic disturbances: The unsteady Kutta condition. *AIAA Journal* **24** (2), 193–199.
- [33] POLING, D. R. & TELIONIS, D. P. 1987 The trailing edge of a pitching airfoil at high reduced frequency. *ASME Journal of Fluids Engineering* **109** (4), 410–414.
- [34] POZRIKIDIS, C. 2000 Theoretical and computation aspects of the self-induced motion of three-dimensional vortex sheets. *Journal of Fluid Mechanics* **425**, 335–366.
- [35] POZRIKIDIS, C. 2009 *Fluid dynamics. Theory, Computation, and Numerical Simulation*, 2nd edn. Springer US.
- [36] PULLIN, D. I. 1978 The large-scale structure of unsteady self-similar rolled-up vortex sheets. *Journal of Fluid Mechanics* **88** (3), 401–430.
- [37] ROSENHEAD, L. 1931 The formation of vortices from a surface of discontinuity. *Proceedings of the Royal Society A: Mathematical, Physical and Engineering Sciences* **134** (823), 170–192.
- [38] ROTT, N. 1956 Diffraction of a weak shock with vortex generation. *Journal of Fluid Mechanics* **1**, 111–128.
- [39] SAFFMAN, P. G. 1992 *Vortex Dynamics*. Cambridge, UK: Cambridge University Press.
- [40] SARPKAYA, T. 1975 An inviscid model of two-dimensional vortex shedding for transient and asymptotically steady separated flow over an inclined plate. *Journal of Fluid Mechanics* **68**, 109–128.
- [41] SEARS, W. R. 1956 Some recent developments in airfoil theory. *Journal of the Aeronautical Sciences* **23** (5), 490–499.

- [42] WAGNER, H. 1925 Über die Entstehung des dynamischen Auftriebes von Tragflügeln. *Journal of Applied Mathematics and Mechanics* **5** (1), 17–35.
- [43] WANG, C. & ELDREDGE, J. D. 2013 Low-order phenomenological modeling of leading-edge vortex formation. *Theoretical and Computational Fluid Dynamics* **27** (5), 577–598.
- [44] WESTWATER, F. L. 1935 The rolling up of a surface of discontinuity behind an aerofoil of finite span. Report R&M 1692. Aeronautical Research Council.
- [45] WU, J-Z., MA, H-Y. & ZHOU, M-D. 2006 *Vorticity and vortex dynamics*. Springer.
- [46] XIA, X. & MOHSENI, K. 2013 Lift evaluation of a two-dimensional pitching flat plate. *Physics of Fluids* **25** (9), 091901(1–26).
- [47] XIA, X. & MOHSENI, K. 2017 Unsteady aerodynamics and vortex-sheet formation for a two-dimensional airfoil. *Journal of Fluid Mechanics* **830**, 439–478.
- [48] XU, L. 2016 Numerical study of viscous starting flow past wedges. *Journal of Fluid Mechanics* **801**, 150–165.